(12)

DNA 4806T-4

MISERS BLUFF ELECTROMAGNETIC PROPAGATION EXPERIMENTS

Final Analysis of the Laser Experiment Data

A. Rosengreen
A. Burns
SRI International
333 Ravenswood Avenue
Menlo Park, California 94025

1 October 1980

Topical Report for Period 26 February 1979—30 June 1980

CONTRACT No. DNA 001-79-C-0181

APPROVED FOR PUBLIC RELEASE;
DISTRIBUTION UNLIMITED.

THIS WORK SPONSORED BY THE DEFENSE NUCLEAR AGENCY
UNDER RDT&E RMSS CODE B322079462 I25AAXHX68503 H2590D.

Prepared for
Director
DEFENSE NUCLEAR AGENCY
Washington, D. C. 20305

UNCLASSIFIED

SECURITY CLASSIFICATION OF THIS PAGE (When Data Entered)

REPORT DOCUMENTATION PAGE		READ INSTRUCTIONS BEFORE COMPLETING FORM
1. REPORT NUMBER DNA 4806T-4	2. GOVT ACCESSION NO. AD-A092	3. RECIPIENT'S CATALOG NUMBER 425
4. TITLE (and Subtitle) MISERS BLUFF ELECTROMAGNETIC PROPAGATION EXPERIMENTS Final Analysis of the Laser Experiment Data		5. TYPE OF REPORT & PERIOD COVERED Topical Report for period 26 Feb 79 — 30 Jun 80 6. PERFORMING ORG. REPORT NUMBER SRI Project 8279
7. AUTHOR(s) Arne Rosengreen Alan A. Burns		8. CONTRACT OR GRANT NUMBER(s) DNA 001-79-C-0181
9. PERFORMING ORGANIZATION NAME AND ADDRESS SRI International 333 Ravenswood Avenue Menlo Park, California 94025		10. PROGRAM ELEMENT, PROJECT, TASK AREA & WORK UNIT NUMBERS Subtask I25AAXHX68503
11. CONTROLLING OFFICE NAME AND ADDRESS Director Defense Nuclear Agency Washington, D.C. 20305		12. REPORT DATE 1 October 1980 13. NUMBER OF PAGES 50
14. MONITORING AGENCY NAME & ADDRESS(if different from Controlling Office)		15. SECURITY CLASS (of this report) UNCLASSIFIED 15a. DECLASSIFICATION/DOWNGRADING SCHEDULE N/A

16. DISTRIBUTION STATEMENT (of this Report)

Approved for public release; distribution unlimited.

17. DISTRIBUTION STATEMENT (of the abstract entered in Block 20, if different from Report)

18. SUPPLEMENTARY NOTES

This work sponsored by the Defense Nuclear Agency under RDT&E RMSS Code B322079462 I25AAXHX68503 H2590D.

19. KEY WORDS (Continue on reverse side if necessary and identify by block number)

MISERS BLUFF
Nuclear Weapons Effects
Dust and Debris
Electromagnetic Propagation
Laser Systems

20. ABSTRACT (Continue on reverse side if necessary and identify by block number)

This report describes the lidar data obtained at 1.06 and 0.53 μm during the MISERS BLUFF II-2 (MBII-2) tests at the Planet Test Site near Lake Havasu City, Arizona. Experiments were also performed at 10.6 μm, but data from these experiments were lost because the recording system malfunctioned. The results from the first four minutes after the detonation are presented. In retrospect, the theoretical analysis, which was developed before the data was ready for final reduction, was of limited use because of the unexpected —

DD FORM 1 JAN 73 1473 EDITION OF 1 NOV 65 IS OBSOLETE

UNCLASSIFIED

SECURITY CLASSIFICATION OF THIS PAGE (When Data Entered)

nature of the cloud echoes. The 2.5-MHz receiver bandwidth provided insufficient resolution for the signals that were returned from a region that extended at most only a few tens of meters into the cloud. For the most part, laser signals did not penetrate very deeply into the cloud. Average values for the volume backscattering coefficient have been calculated for the first two minutes after the detonation. They range from 2 to 9 · 10^{-2} m^{-1} sr^{-1} at 0.53 μm and 3 to 15 · 10^{-3} m^{-1} sr^{-1} at 1.06 μm. The corresponding reflectance values, if the cloud is treated as a rough-surfaced solid object, range from 9 to 42 percent and 1.4 to 7 percent, respectively, which are close to values observed from actual solid surfaces that scatter diffusely. The dependence on wavelength suggests that the scattering was caused predominantly by particles of submicron size. In general, the results show that lidar measurements provide little information about the formation of dust clouds as dense as that present at MBII-2. These measurements suggest that dust clouds produced by nuclear and large conventional explosions act as rough-surfaced solid objects in their effects on laser-based systems.

TABLE OF CONTENTS

LIST OF ILLUSTRATIONS

I INTRODUCTION

The continuing development of the laser technology has resulted in a proliferation of laser-guided weapons in the visible and the infrared (IR) ranges of the spectrum. So far, the performance of these weapons in both the conventional and the nuclear dust environments is not well understood. To increase the knowledge in this area, SRI International performed measurements using a three-wavelengths (0.53, 1.06, and 10.6 μm) autotracking lidar at the two MISERS BLUFF II (MBII) High-Explosive Tests, to determine the volume backscatter and extinction coefficients of the explosion-produced dust cloud. To this end, two-way transmission and backscatter radiation measurements were attempted. Such measurements allow not only an evaluation of the system performance, but also an evaluation of the cloud formation and the distribution of particle size.

The three wavelengths used in the experiment (Figure 1) are representatives of those designators, range finders and lasers proposed or existing in military systems.

The laser experiment was one of four experiments fielded by SRI for MBII. The other three involved measurement of scattering and transmission effects in the HF, UHF, SHF, and EHF bands. These experiments and their preliminary results are described and discussed in earlier reports.[1,2]*

*All references are listed at the end of the report.

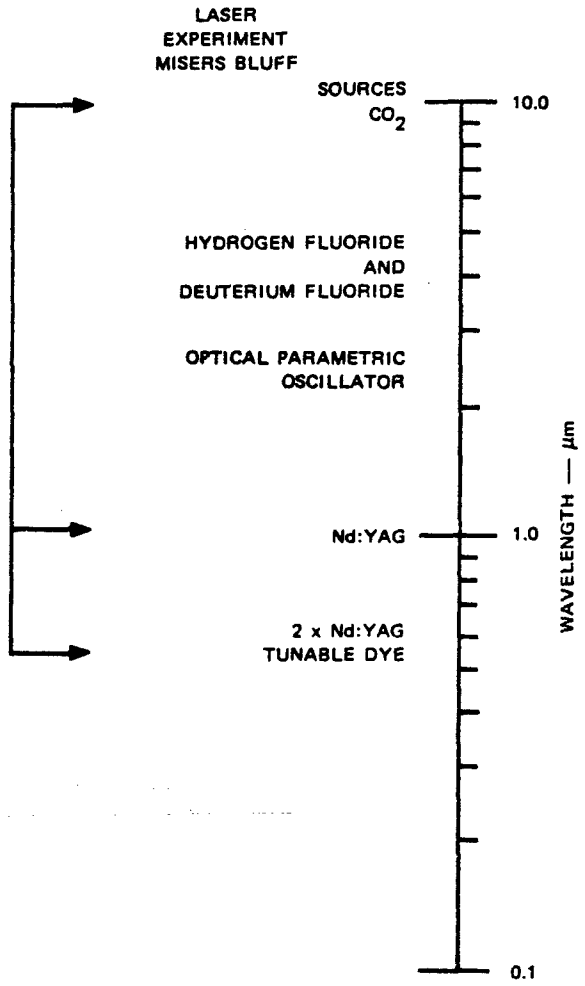

FIGURE 1 OPTICAL WAVELENGTHS RELEVANT TO PROJECT MISERS BLUFF

Both MISERS BLUFF II (MBII-1 and MBII-2) tests took place at the Planet Ranch test site on the dry bed of the Bill Williams River, Lake Havasu City, Arizona. The location of the radar/laser vans is shown in the lower left corner of the map in Figure 2. The first test, MBII-1, which was a 120-ton ammonium nitrate and fuel oil (ANFO) detonation,

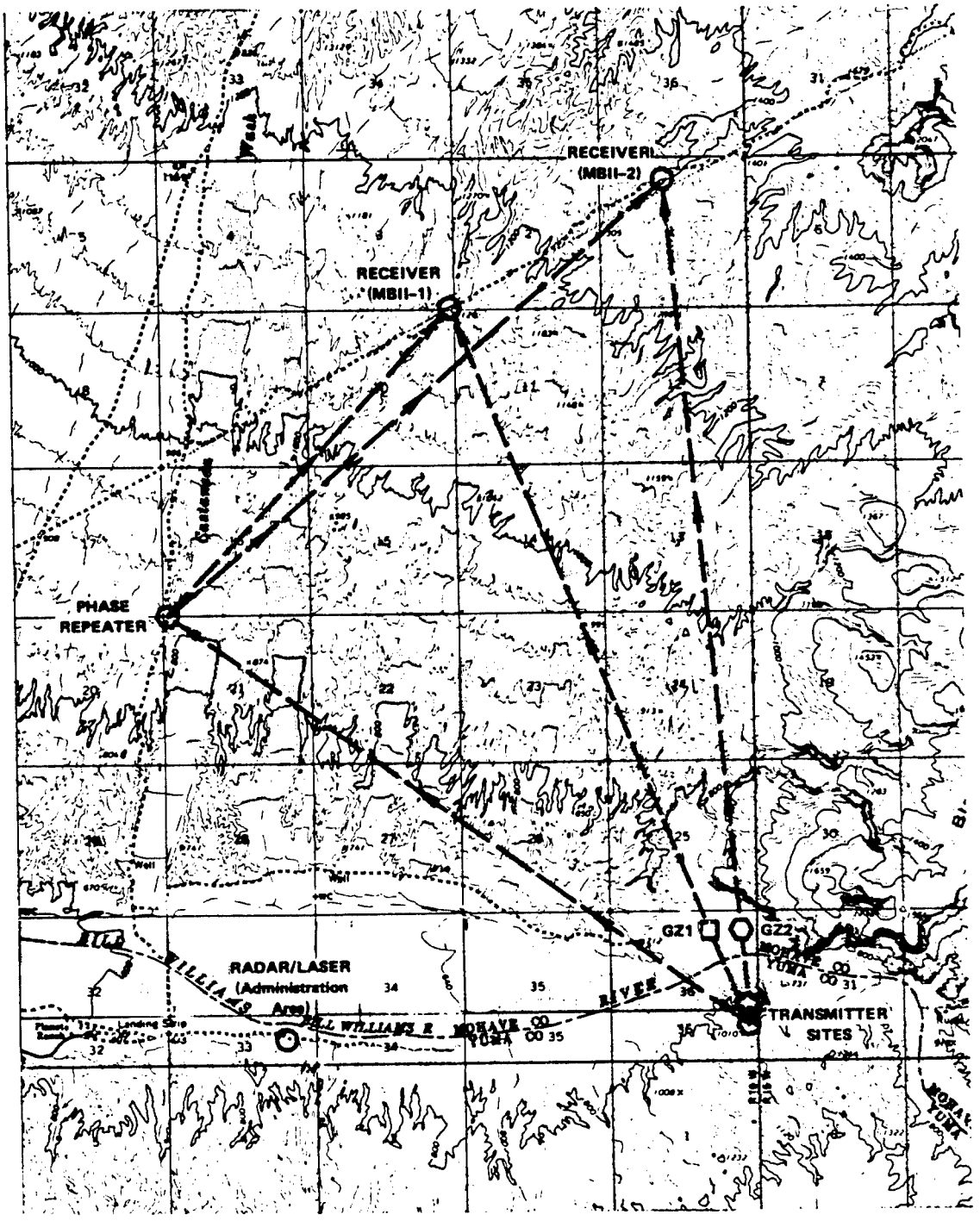

FIGURE 2 POSITIONS OF MISERS BLUFF LASER AND UHF-EHF PROPAGATION EXPERIMENT ELEMENTS

took place at 1300 MST on 28 June 1978. The second test, MBII-2, took place at 1100 MST on 30 August 1978, and consisted of the simultaneous detonation of six such 120-ton ANFO charges uniformly spaced on the periphery of a 100-m-radius circle. Although the primary objective of the MBII tests was the study of ground motion in a multiple-burst environment in support of the MX program, the tests provided a good opportunity to measure dust effects as well. Our experiments were added and were conducted on a noninterference basis along with other activities, which, because they were primarily shock and blast related, were confined to the immediate area around ground zero (GZ).

The experimental geometry was such that GZ of MBII-1 was located on a line between the lidar van and a retroreflector placed on a 365-m bluff. From the observation of the cloud movement caused by the wind during MBII-1, it was decided to retain this arrangement during MBII-2. Thus, because of the slightly different azimuths of the two GZs, the line between the lidar and the retroreflector was slightly offset to the northwest from the GZ of the second event. To extend the time of data collection beyond the time the cloud was between the lidar and the retroreflector, a helicopter was outfitted with a retroreflector and flown behind the cloud several minutes after the detonation.

Hawley and Burns[3] have already presented a description of the lidar system, the techniques used for measuring, and the general range data showing the range of the scattering centers as a function of time. This document is the final report on the analysis and interpretation of the MBII laser experiment data. Because of equipment difficulties and adverse wind conditions during MBII-1, the MBII-2 data were very much superior (although there were problems with the hardware then as well); therefore, to gain the most from the analysis effort, we concentrated entirely on the larger MBII-2 event. Because of the close proximities of the two GZs, the soil and cloud properties (other than the size of the cloud) of the two events are likely to be very similar to one another. Thus, the results of the MBII-2 analysis that are presented here should also apply equally well to the MBII-1 test.

This report is organized as follows: In Section II is an evaluation of system performance. Section III is a theoretical exposition of concepts that provide a background for the data analysis. Section IV contains the data. Section V contains the analysis of the data. Section VI is the conclusion and summary.

II EVALUATION OF THE SYSTEM PERFORMANCE

The data that are used in this and the following sections were recorded during MBII-2 as explained in the Introduction.

Before MBII-2, the lidar system was checked by firing each laser separately for a certain length of time. Based on these tests, both the lasers, the receivers, and the data-acquisition system appeared to function normally. However, during MBII-2 when the video data switch in Figure 3 (for more information about the instrumentation in this figure see Hawley and Burns[3]) was operating between the three receiver outputs synchronously with the firing of the lasers, the stored data show that part of the data was perturbed. Besides the receiver signals, which were stretched using a Gaussian filter and then sampled every 0.1 μs, the data consist of several status words (SW), of which three contain information about the wavelength and the data from the laser energy monitors and the azimuth/elevation (Az/El) monitor shown in Figure 3. The wavelength information is found in SW No. 3; SW No. 4 stores in alternating order the azimuth (Az) and elevation (El) of the telescope. SW No. 5 lists the energy of the transmitted laser pulse. Of these three words, only SW No. 3 appears reasonably reliable (about 80 percent). The data of the other words appear to have been perturbed. Although the data of SW No. 4 show some indication of alternating between two values, all attempts to recover the data by bit inversion or permutation of the bit positions have failed. The data in SW No. 4 show no change even though the receiver data show clearly that the telescope direction was changed (during the experiments with the moving retroreflector on the helicopter). This lack of correlation is sufficient reason to consider the Az/El data lost. We have reached a similar conclusion for the data contained in SW No. 5 because we were not able to get them to match with the expected laser output energies.

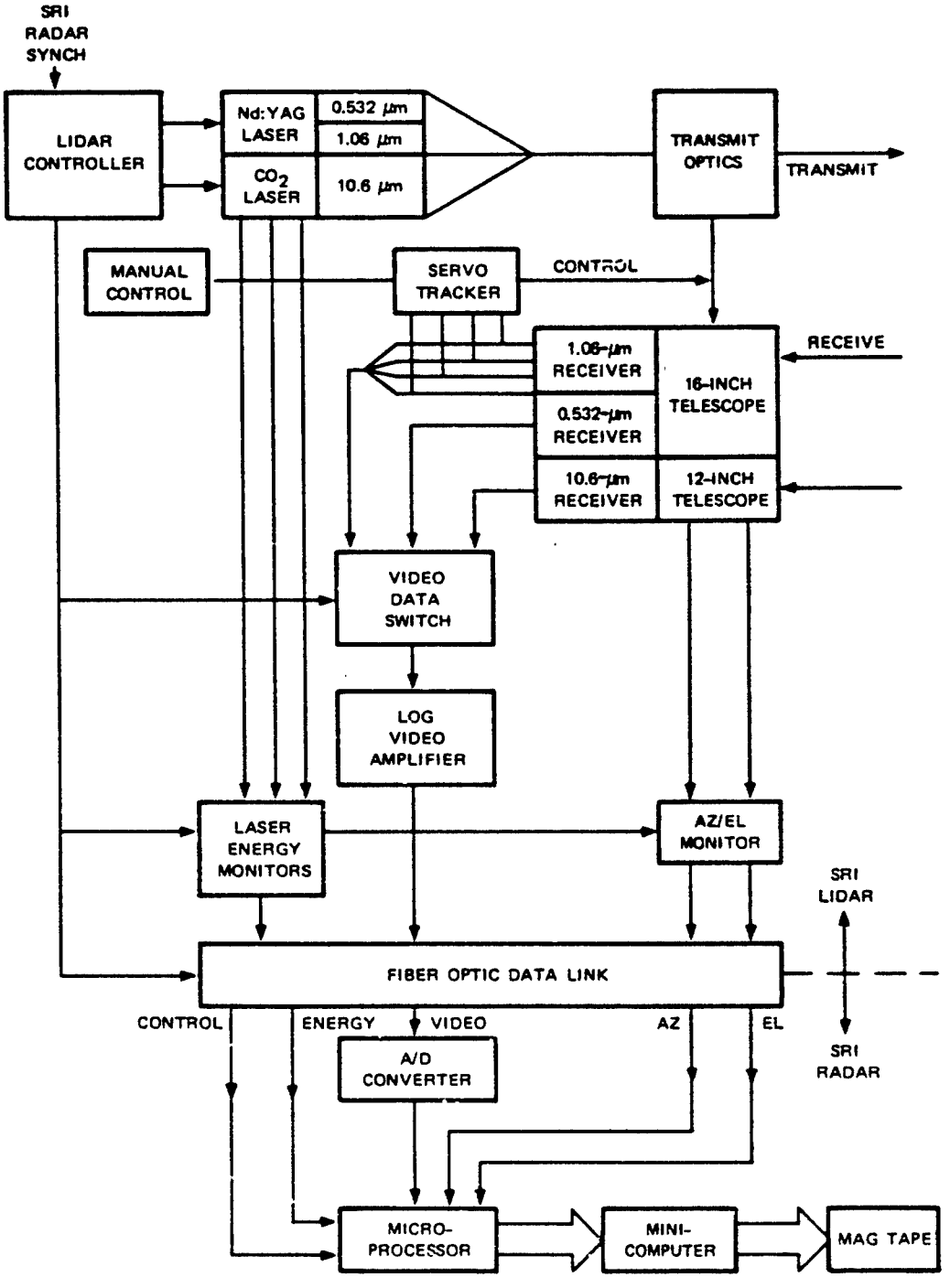

FIGURE 3 LASER EXPERIMENT SYSTEM BLOCK DIAGRAM

All 10.6-μm data were lost as well. The data acquisition system was designed to record the 1.06- and 0.53-μm receiver outputs on alternate 10-pps Nd:YAG laser shots, except every tenth pulse when the slower (1-pps) CO_2 laser fired. But when the recordings were carefully inspected, we found that the preceding 0.53-μm data were repeated where the 10.6-μm output should have been.

The source of the problems appears to be in the video data switch and associated circuitry. Examination of the wiring diagrams does not provide any clues to the exact cause of the problems. A full understanding of the failure requires an examination of the actual system, an exercise of little value at this point.

The lidar system was calibrated by recording the return signal from a white target located at a distance of approximately 1 km from the lidar van. Figures 4 and 5 show the relative return signal at 0.53 and 1.06 μm, respectively. The return near the origin is caused by near scattering and is most pronounced at 0.53 μm. Comparison of the near-scattering signal in Figure 4 with those obtained on the oscilloscope show that the time in Figures 4 and 5 should be increased by about 0.5 μs placing the return from the target at 6.6 μs, corresponding to a distance of 990 m.

The receiver response to the 10-ns laser pulse reflected by the calibration target is basically the much wider receiver impulse response. To remove the distortion present in Figures 4 and 5 because of the log scale, we have plotted the impulse responses on a linear scale in Figure 6. A half width of slightly less than 0.2 μs for the 0.53-μm receiver agrees reasonably well with the impulse response of a receiver band limited by a Gaussian filter with a 3-dB bandwidth of 2.5 MHz. The impulse response of the 1.06-μm receiver is a little more difficult to evaluate because the sampling time is such that it truncates the receiver signal. It is obvious, however, that the 1.06-μm signal is much wider than that at 0.53 μm. We believe that the relatively slow fall time is caused by a long tail of the Nd:YAG laser pulse. Although this laser was also used to generate the pulse at 0.53 μm by a second harmonic generation, the

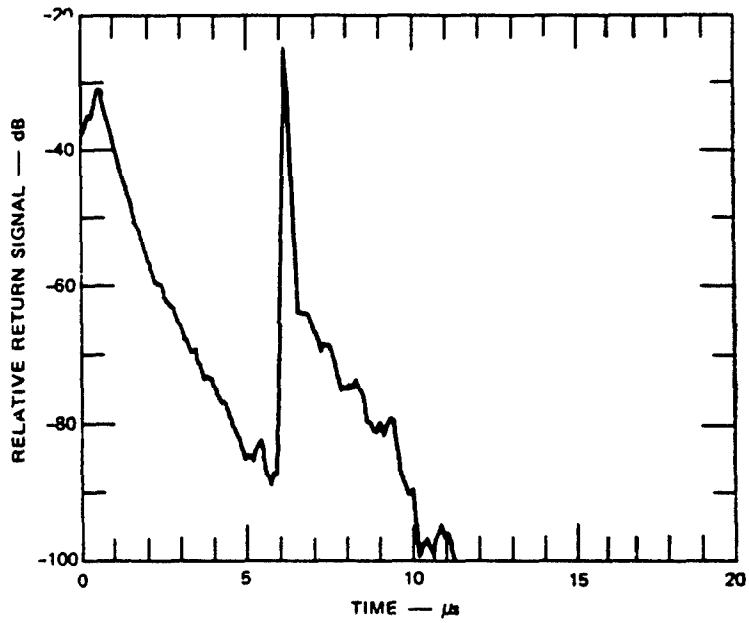

FIGURE 4 CALIBRATION DATA AT 0.53 μm

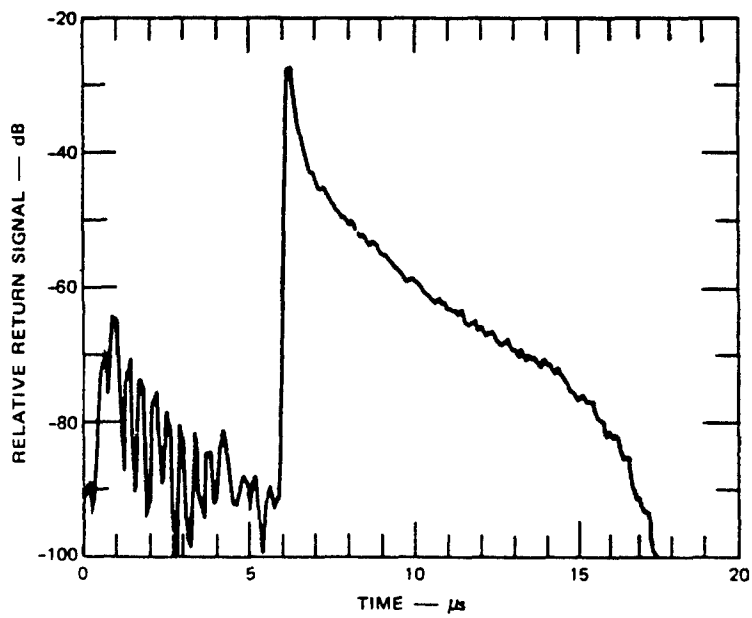

FIGURE 5 CALIBRATION DATA AT 1.06 μm

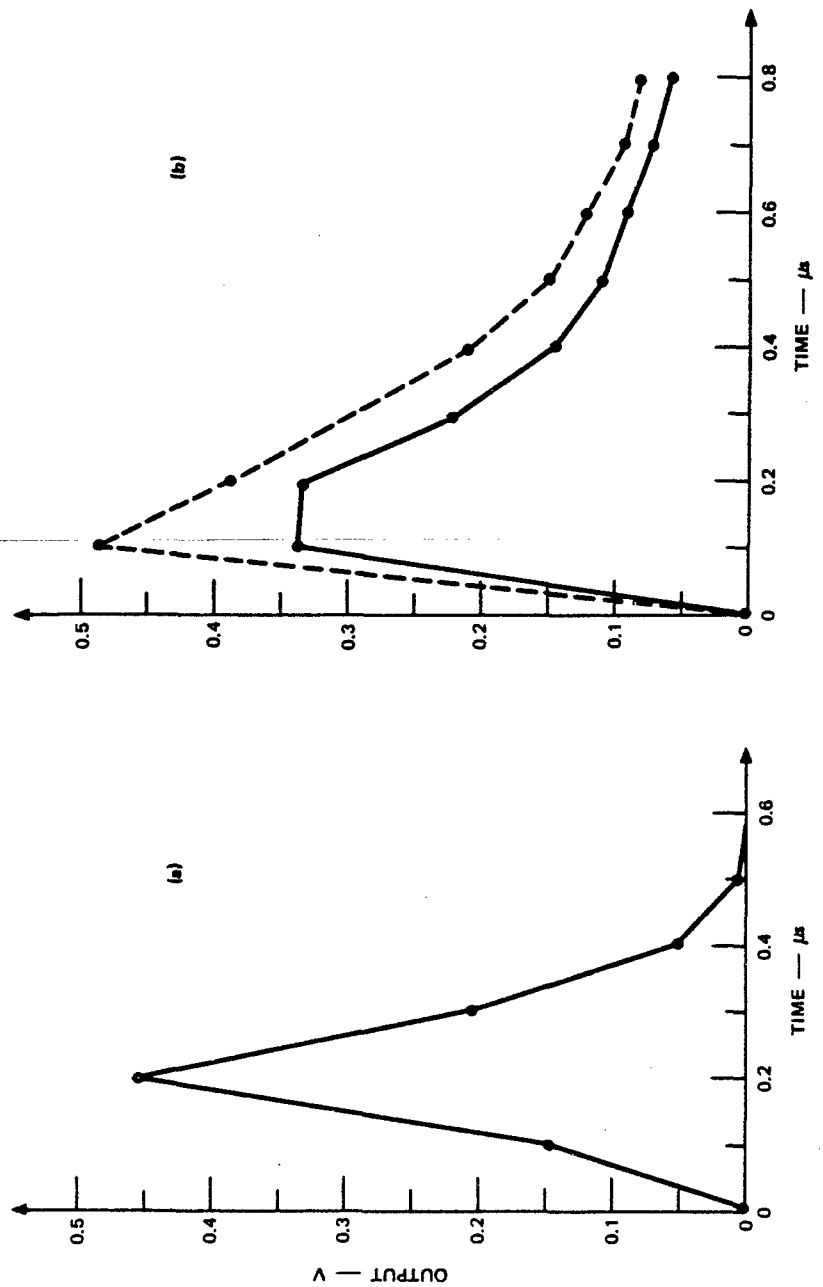

FIGURE 6 IMPULSE RESPONSE OF LIDAR RECEIVERS

pulse at 0.53 μm does not show any pronounced tail because the efficiency of the second harmonic generation is proportional to power. Based on the half width of the pulses in Figure 4, the resolution of the lidar system is about 30 m at 0.53 μm and about 60 m at 1.06 μm.

The rms fluctuation of the return signal, based on 80 returns, is in terms of percentage of the mean, 10.8 percent at 1.06 μm and 17.6 percent at 0.53 μm. These figures agree well with the expected fluctuation of the laser output power. Because of the loss of data from the laser output monitor, the figures present the basic limitation of the accuracy of the collected data.

III THEORETICAL ANALYSIS

In the following we develop a simple theory for the backscattered radiation that allows calculation of the volume backscatter coefficient from the lidar data in the presence of attenuation of the laser signal by the dust cloud. It is based on the lidar equation given by:[4]

$$P_r(R) = \frac{P_t}{\Omega R^2}\,\sigma(R)\,\frac{A_r}{4\pi R^2}\,\exp\left[-2\int_0^R \alpha(r)dr\right] T_0 \qquad (1)$$

that expresses the power received, $P_r(R)$, by the lidar system from a scattering event at a distance, R, in terms of the following parameters:

P_t = transmitted energy
Ω = solid angle of transmitted laser beam
$\sigma(R)$ = scattering cross section
A_r = receiver aperture
$\alpha(r)$ = extinction coefficient
r = variable of integration
T_o = transmittance of optical receiver.

In Eq. (1) it is assumed that:

(a) Only a single scattering event takes place.

(b) The energy is scattered uniformly over the entire 4π solid angle.

(c) The scattering area is larger than the cross-sectional area of the laser beam at the scattering medium.

The assumptions (a) and (b) simplify the theory greatly and are reasonable in view of the lack of any a priori information about the details of the scattering process. As more information is obtained more sophisticated models can be applied later.

To conform to the standard notation, we introduce the volume backscattering coefficient $\beta(R)$ given by:

$$\beta(R) = \frac{\sigma(R)}{4\pi\left(\frac{c\tau}{2}\Omega R^2\right)} \tag{2}$$

where c is the speed of light and τ is the length of the laser pulse. The factor $c\tau/2\Omega R^2$ is the scattering volume that contributes to the received lidar signal at a fixed time, and 4π is the total solid angle. Thus, the dimension of $\beta(R)$ is $m^{-1}sr^{-1}$. Inserting Eq. (2) in Eq. (1) we obtain:

$$P_r(R) = P_t \left(\frac{c\tau}{2}\right) \beta(R) \frac{A_r}{R^2} \exp\left[-2\int_0^R \alpha(r)dr\right] T_o \tag{3}$$

Before we find $\beta(R)$ from Eq. (3), we normalize $P_r(R)$ with respect to the received power, $P_r(R_{cal})$, measured during the calibration of the lidar system. The calibration consisted of measuring the signal returned from a white sheet of known reflectance placed a distance, R_{cal}, from the lidar van. The received power is given by:

$$P_r\left(R_{cal}\right) = P_t \frac{A_r \rho}{\pi R_{cal}^2} T_a^2\left(R_{cal}\right) T_o \tag{4}$$

where ρ is the reflectance of the calibration target and $T_a^2\left(R_{cal}\right)$ is the two-way transmittance to the target given by:

$$T_a^2\left(R_{cal}\right) = \exp\left[-2\int_0^{R_{cal}} \alpha(r)dr\right] \quad . \tag{5}$$

The subscript, a, has been added to indicate that the transmittance is that of air over the specified range. Eq. (4) takes into account that the beam diameter at the target is smaller than the target and that the

illuminated target area is within the field of view of the receiver. The expression also assumes that the reflection of the target is Lambertian.

By using Eq. (4), the normalized version of Eq. (3) takes the form,

$$P_r(R)/P_r\left(R_{cal}\right) = \frac{\beta(R)}{\beta_o}\left(\frac{R_{cal}}{R}\right)^2 T^2\left(R,R_{cal}\right) \tag{6}$$

where we have used the notation,

$$T^2\left(R,R_{cal}\right) = \exp\left[-2\int_{R_{cal}}^{R} \alpha(r)dr\right] \quad . \tag{7}$$

The backscattering coefficient in Eq. (6) has been normalized with respect to the equivalent backscattering coefficient of the calibration target, β_o, given by

$$\beta_o = \frac{2\rho}{c\tau\pi} \quad . \tag{8}$$

In addition to the unknown, $\beta(R)$, that we wish to find, Eq. (6) contains via Eq. (7), another unknown, the extinction coefficient, $\alpha(r)$. To circumvent this problem we shall use the customary assumption[3] that extinction is proportional to scattering as expressed by:

$$\alpha(R) = k\beta(R) \tag{9}$$

where k is a proportionality constant. Using this relationship in Eq. (6) we obtain by rearrangement of some of the terms the following integral equation for $\beta(R)$:

$$x(R) = \beta(R)\ \exp\left[-2k\int_{R_o}^{R} \beta(r)dr\right] \tag{10}$$

where

$$x(R) = \beta_o \frac{P_r(R)}{P_r\left(R_{cal}\right)} \left(\frac{R}{R_{cal}}\right)^2 T_a^{-2}\left(R_o, R_{cal}\right) \quad . \tag{11}$$

In Eqs. (9) and (10) we have assumed that the scattering events start at R_o, the beginning of the dust cloud. The factor, β_o, is the equivalent backscattering coefficient of the calibration target. By differentiating both sides of Eq. (10) and dividing by x/β, Eq. (10) can, after rearrangement of the terms, be written

$$\frac{d\beta(R)}{dR} = \frac{dx(R)}{x(R)dR}\beta(R) + 2k\beta^2(R) \quad . \tag{12}$$

This is the "Riccati" equation. The details of the solution of this equation are given in Appendix A. The solution is

$$\beta(R) = \frac{\frac{P_r(R)}{P_r(R_o)}\left(\frac{R}{R_o}\right)^2}{1/\beta(R_o) - 2k\int_{R_o}^{R} \frac{P_r(r)}{P_r(R_o)}\left(\frac{r}{R_o}\right)^2 dr} \quad , \tag{13}$$

which is similar to the expression given by Davis[5].

Although we eliminated $\alpha(R)$ by using the relation in Eq. (9), the problem of finding the proportionality factor, k, still remains. To solve this problem we follow the approach of Fernald, et al.[6], who showed that k can be obtained from transmittance measurements.

The general expression for the two-way transmittance is given by the exponential term in Eq. (1). If we used the relationship between the extinction coefficient and the backscattering coefficient in Eq. (9) the transmittance can be written as

$$T^2(R) = \exp\left[-2k\int_o^R \beta(r)dr\right] \quad . \tag{14}$$

By differentiating this equation with respect to R and inserting the result in Eq. (6) we obtain, after a few mathematical manipulations, which are described in Appendix B, the following expression for k:

$$k = \frac{1 - T_a^2\left(R_1, R_o\right) \frac{P_r(R_2)}{P_{r,a}(R_2)}}{2\beta_o T^2\left(R_{cal}\right) \int_{R_o}^{R_1} \frac{P_r(r)}{P_r\left(R_{cal}\right)} \left(\frac{r}{R_{cal}}\right)^2 dr} \tag{15}$$

where $R_o \leq R \leq R_1$ is the range of the cloud, R_2 the distance to the retroreflector and $P_{r,a}(R_2)$ the power received from the retroreflector when no cloud is present.

The remaining factor to be discussed in the expression for $\beta(R)$ is $\beta(R_o)$, the value of $\beta(R)$ at the front edge of the cloud. It is found by setting $R = R_o$ in Eq. (6) and is given by

$$\beta_o(R_o) = \beta_o \frac{P_r(R_o)}{P_r\left(R_{cal}\right)} \left(\frac{R_o}{R_{cal}}\right)^2 T_a^{-2}\left(R_o, R_{cal}\right) \quad . \tag{16}$$

It assumes that the effect of the scattering on the transmittance of the first small increment of the cloud is negligible.

IV PRESENTATION AND DISCUSSION OF THE DATA

In the following we show a sequence of figures covering the first four minutes of MBII-2. To help in the interpretation of the data we present Figure 7, which shows the approximate position of the laser beam projection in the GZ plane in relation to the detonation charges,

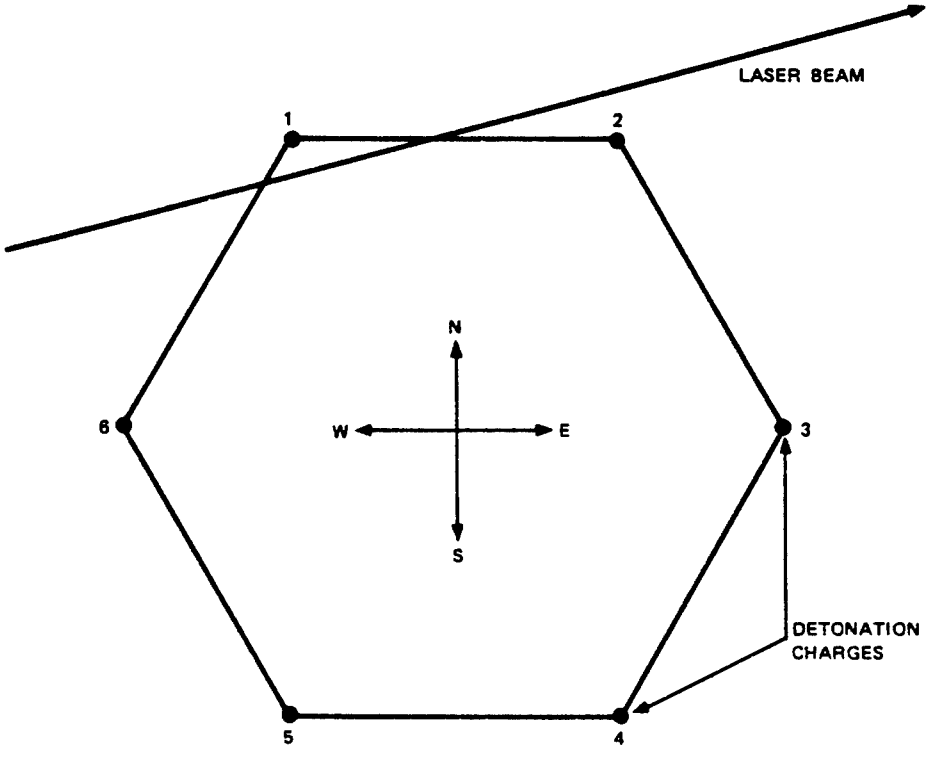

FIGURE 7 PROJECTION OF LASER BEAM ON THE GROUND-ZERO PLANE

and Figure 8, which is an overhead photograph of the GZ area slightly after detonation. The latter figure shows that during this early stage of the detonation six separate dust clouds are formed centered around the positions of each of the explosive charges.

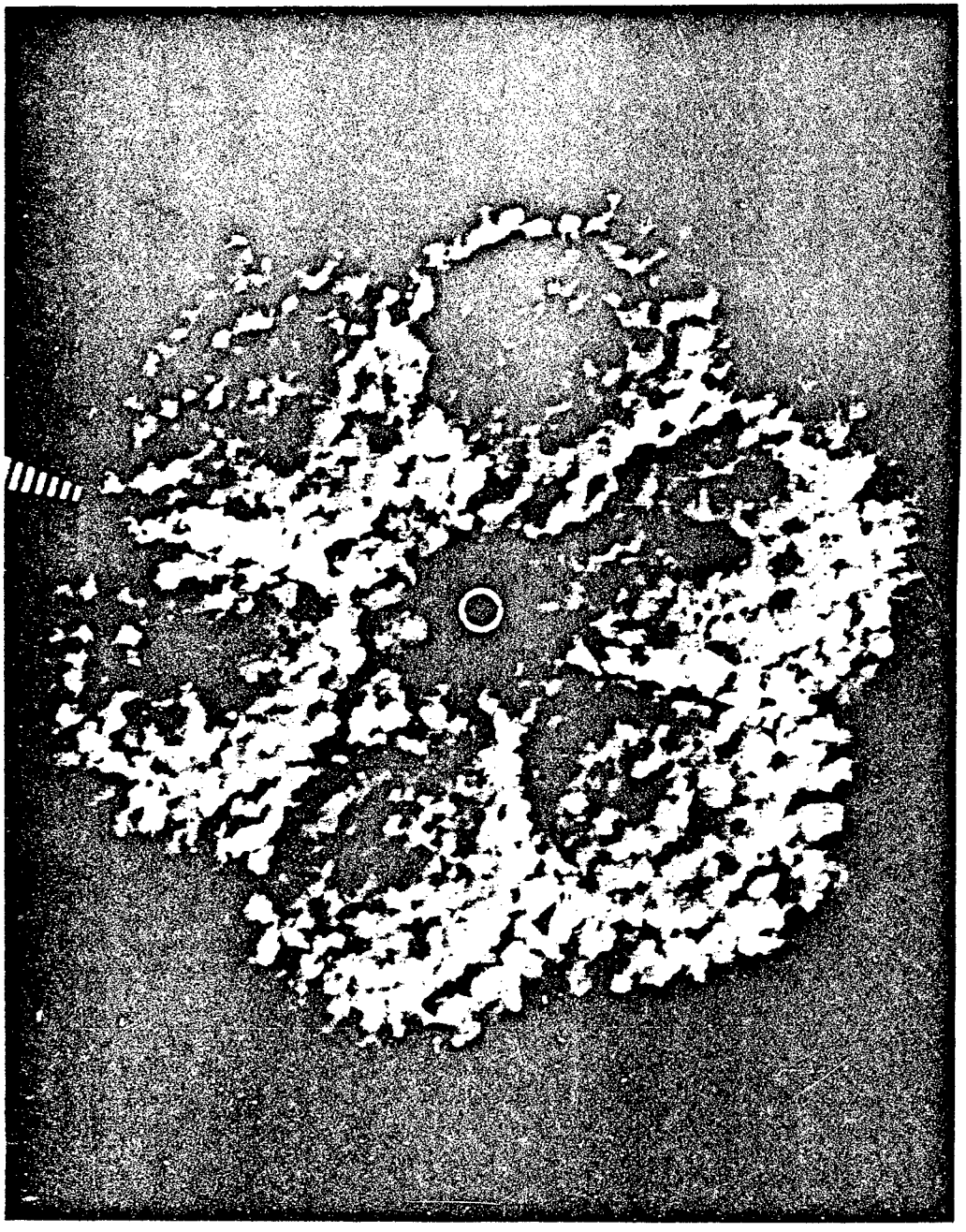

FIGURE 8 OVERHEAD PHOTOGRAPH OF GROUND ZERO AT AN EARLY STAGE OF THE DETONATION

The presence and development of these separate clouds are shown clearly in the lidar data (Figure 9). The data shown are for 0.53 μm. Figure 9(a) shows the first intercept of the laser beam by the two clouds that formed around the two detonation charges (No. 1 and 2) close to the laser beam projection as shown in Figure 7. The ranges are 4.83 and 4.98 km, respectively. The signal close to 6.0 km is the return from the retroreflector. In Figure 9(b) this signal is greatly attenuated; and it is completely obliterated in Figure 9(c) and the following figures; and it reappears three minutes later. Figures 9(b) to 9(e) show the growth of the front cloud and its effect on the return from the cloud behind it. At T + 14.047 s the clouds from the two detonation charges have merged completely and are so dense that the return is limited to a thin layer of dust at the front edge of the cloud associated with charge No. 1.

Further development is depicted by Figures 10(a) through 10(i), and 11(a) through 11(e), which show the return signal every 15 s. The sequence is broken during the period from T + 2 min to T + 2 min 36 s because of a transient computer malfunction that required restarting the data-acquisition program. The figures show that the returns are limited to a few thin layers in the range from 4.7 to 5.0 km. Any radiation propagating beyond that range either was absorbed totally or was scattered out of the receiver field of view until T + 3 min when the return from the retroreflector reappears. This occurred when the main part of the cloud drifted out of the line of sight. Examination of a tape from a TV monitor covering the field of view of the lidar telescope shows that during the time when the return from the retroreflector was observed a faint haze was present, suggesting the presence of fine particles.

During the time the data in Figures 9(a) to 11(c) were taken the dust cloud drifted slowly in a north-northwesterly direction, a direction essentially perpendicular to that of the laser beam (see Figure 7). Thus, the return signal in the range of 4.7 to 5.0 km appears to be from a thin layer of dust at the front edge of the moving dust cloud.

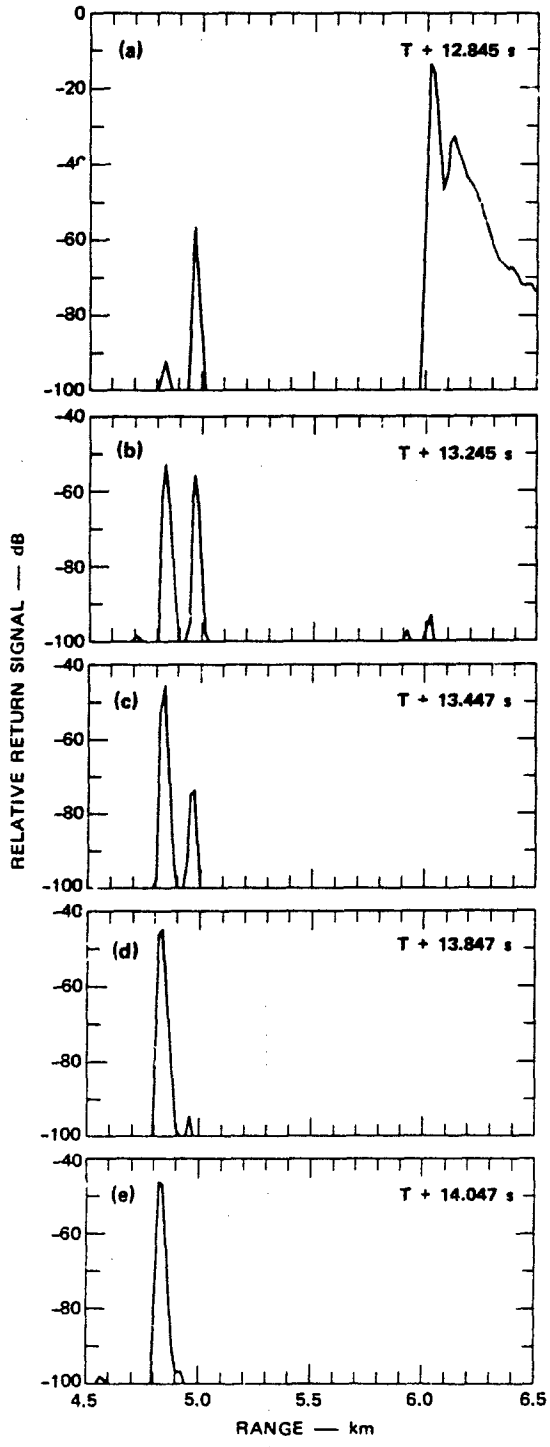

FIGURE 9 LIDAR RETURN AT 0.53 μm vs RANGE

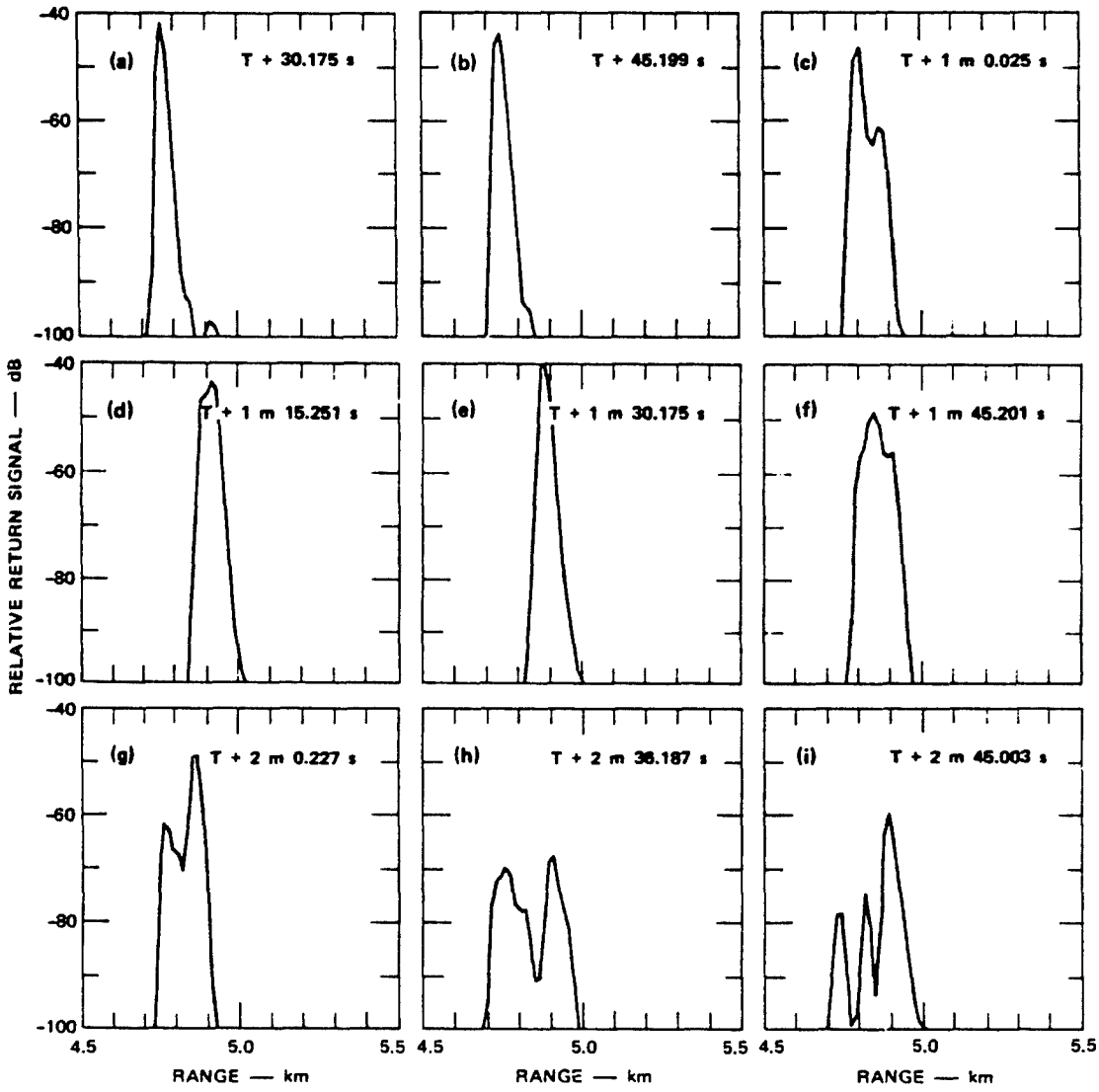

FIGURE .10 LIDAR RETURN AT 0.53 μm vs RANGE

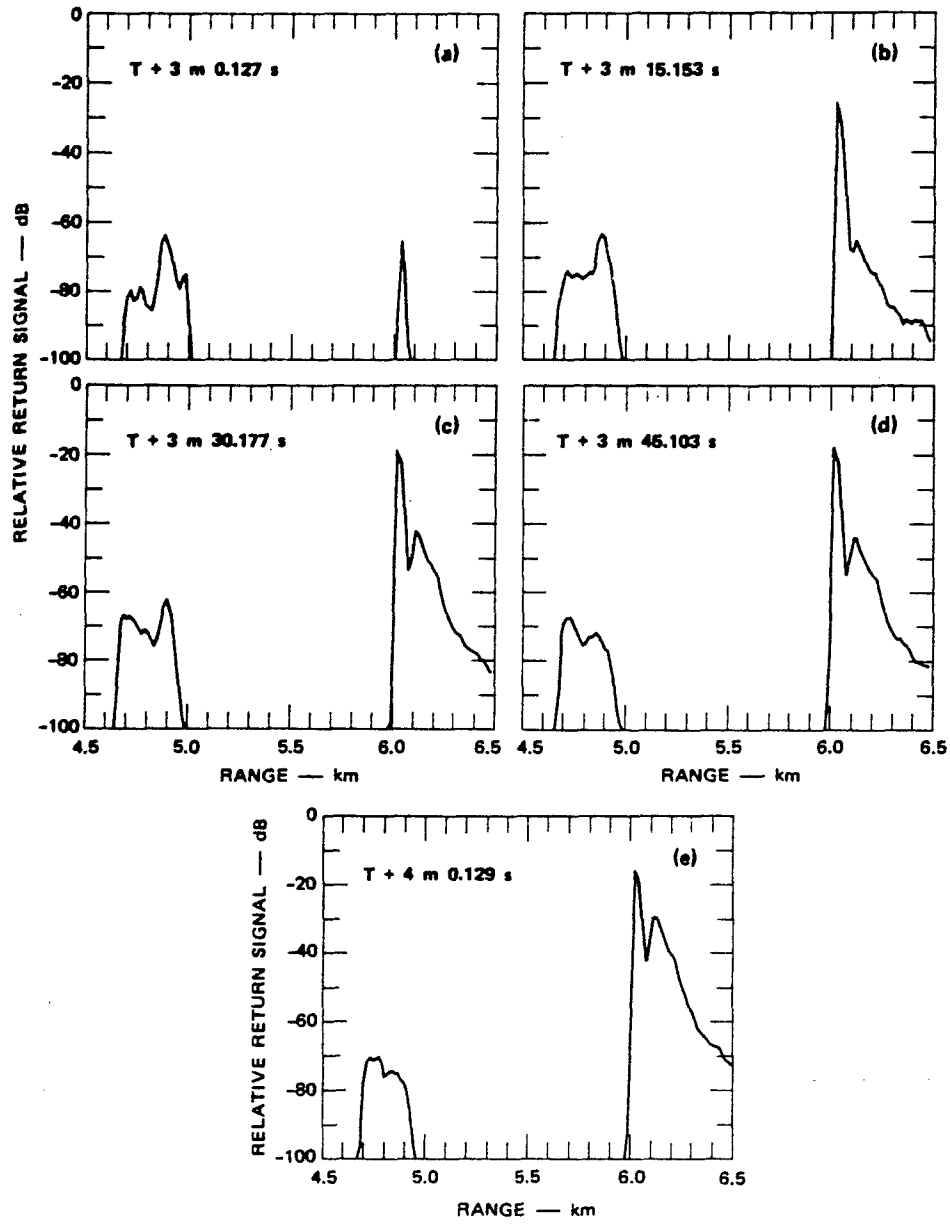

FIGURE 11 LIDAR RETURN AT 0.53 μm vs RANGE

Slightly after T + 4 min the telescope direction was changed to scan the entire cloud. Except for changes of the range, the return signals look similar to those already shown in Figures 9 to 11. Because of the loss of the Az/El data, the data from the scanning experiment do not provide any further information.

After T + 8 min the laser was aimed at a retroreflector dangling below a flying helicopter; however, because of tracking problems, this experiment was not successful. The data that were obtained indicate the presence of small dust pockets in the range from 5 to 15 km. These pockets were small because they moved in and out of the laser beam within 0.2 s when the helicopter was tracked at a distance of 13 km.

The data shown in Figures 9 to 11 are all for 0.53 μm. Corroborating data were obtained at 1.06 μm, but, because of the poorer resolution of the receiver and the smaller backscattering coefficient at that wavelength, the resolution of the data were not as good as those obtained at 0.53 μm. Figures 12(a) to 12(c) show examples of the data at 1.06 μm. They are from the earliest times of the cloud formation, and show the same two peaks, and the disappearance of one of the peaks as shown in Figure 9 for 0.53 μm.

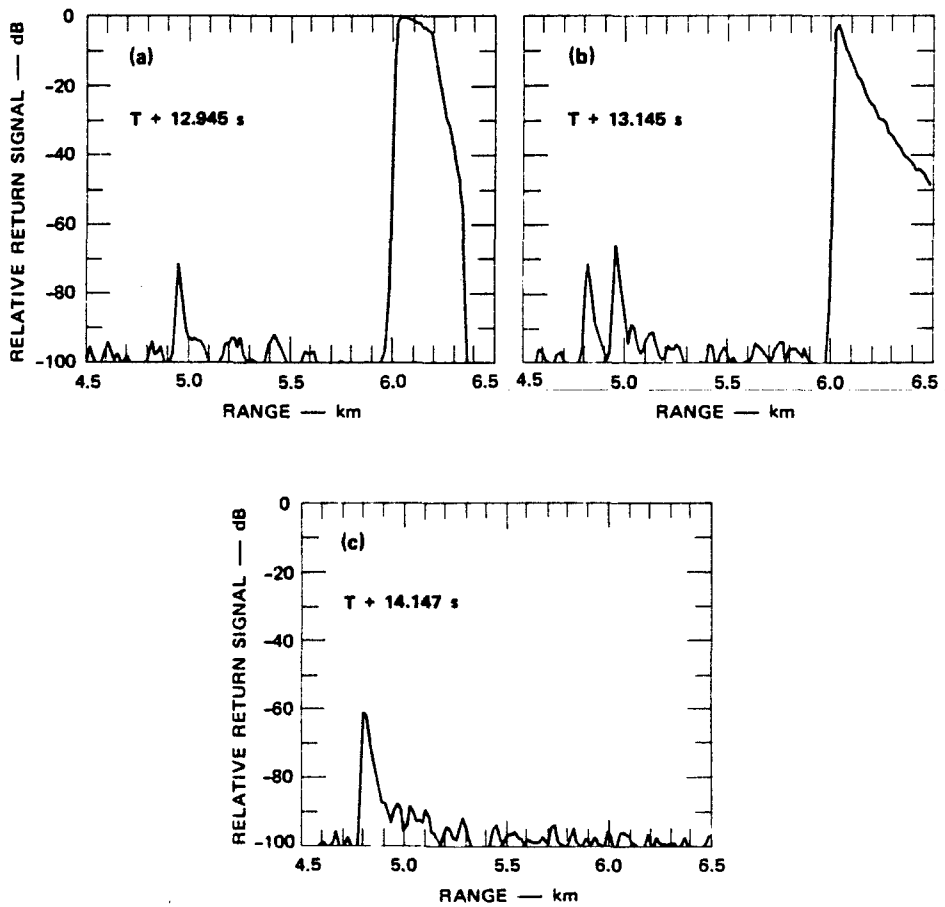

FIGURE 12 LIDAR RETURN AT 1.06 μm vs RANGE

V ANALYSIS OF THE DATA

The data collected during the first four minutes of MBII-2 at the wavelengths 0.53 and 1.06 μm were sufficiently complete to warrant further analysis. The direction for the telescope during that period was fixed and known. Furthermore, because the backscatter coefficient in Eqs. (6) and (13) are expressed in received power relative to that obtained during the calibration, the loss of the data from the laser energy monitor has only a minor effect expressed by the rms fluctuations of the laser output power as discussed in Section II.

The major limitation of the analysis resulted from the great width of the impulse response of the lidar system compared to the short pulse width of the return signal. In reviewing the data in Figures 9 to 11, note that the return signals at the first minute and a half (Figures 9(a) to 10(e)) are identical or very close to the impulse response of the receiver. The impulse response can be seen clearly from the return signal from the retroreflector at the range of 6 km in Figure 9 and Figure 11. In the comparison, remember that because of the logarithmic scale only the upper part of the peaks is important; the tails would not be noticeable in a linear display. As the dust cloud evolves the pulse spreads and often two or more peaks occur that tend to broaden out after T + 3 min.

The only data that seem usable for estimating β from Eq. (13) are the data after T + 3 min, at which time the width of the return pulse is much broader than the impulse response. However, even for those data, the calculations show that the impulse response contributes significantly to the integral in the denominator of the expression for β with the result that $\beta(R)$ becomes a monotonic increasing function of R in the entire range of the cloud from 4.7 to 5.0 km.

As mentioned before, the return signal during the first minute and one half is close to the impulse response of the receiver. This suggests

that the effective scattering region of the cloud is limited to a thin surface layer. If we assume that the layer is infinitely thin, an effective or equivalent volume backscattering coefficient, β, can be found from Eq. (6) by setting the two-way transmittance equal to one and letting the range, R, be the range corresponding to the peak of the return pulse. Because we have assumed an infinitely thin layer, it is perhaps more meaningful in this case to talk about a reflectance. Such a value is obtained easily by multiplying β by the factor $c\tau\pi/2$ (= 4.71 m sr) in Eq. (8). In this case we are comparing the reflectance of the cloud directly with that of the calibration target.

The assumption of an infinitely thin layer is the same as assuming a thin layer with a constant β and a zero extinction coefficient because the range is large compared to the thickness of the layer. Such assumptions are hard to justify if we are interested in the actual value of β, but for the comparison of β at different wavelengths or times, the use of an average value of β seems reasonable.

Even with these assumptions an uncertainty in the calculated value of β remains because during times just after the detonation the return signals have a pulse shape identical or close to that of the receiver impulse response. Thus during that period of time, the actual pulse width of the reflected signal is unknown and could be as short as 10 ns, the width of the laser pulse. From Figure 13, which shows the relative output of the receiver as a function of input pulse width, we see that this introduces an uncertainty factor close to ten. In our calculations we have assumed a pulse width of 200 ns or larger, an assumption that seems reasonable for most of the time interval considered, but an assumption that may result in a value of β that is up to ten times too small immediately after the detonation.

To be able to calculate β from Eq. (6), we must know β_o given in Eq. (8). This implies that we know the reflectance, ρ, of the calibration target. To obtain this value, we compared the return signal from a small sample (about 4 cm x 4 cm) of the target with that from a similarly sized sample consisting of Eastman Kodak white reflectance

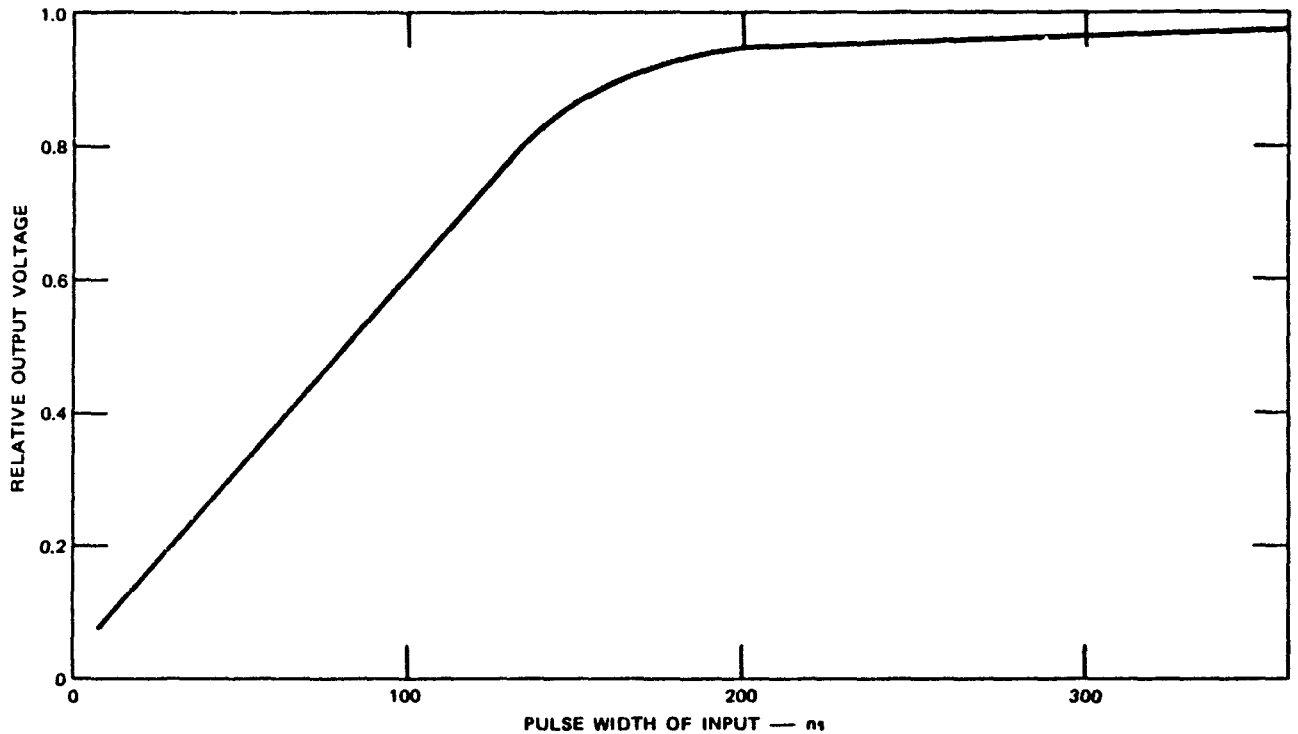

FIGURE 13 RESPONSE OF THE 2.5-MHz FILTER TO SQUARE INPUT PULSES OF DIFFERENT PULSE WIDTHS

coating (No. 6080) on a glass slide. With the beam at normal incidence we were not able to distinguish between the two targets at 1.06 μm. At 0.53 μm the reflectance of the target material used during the calibration appeared to be a few percent lower than that of the Kodak coating. Because the Kodak coating has a known reflectance of better than 0.99 at both 0.53 and 1.06 μm, we can set $\rho = 1$.

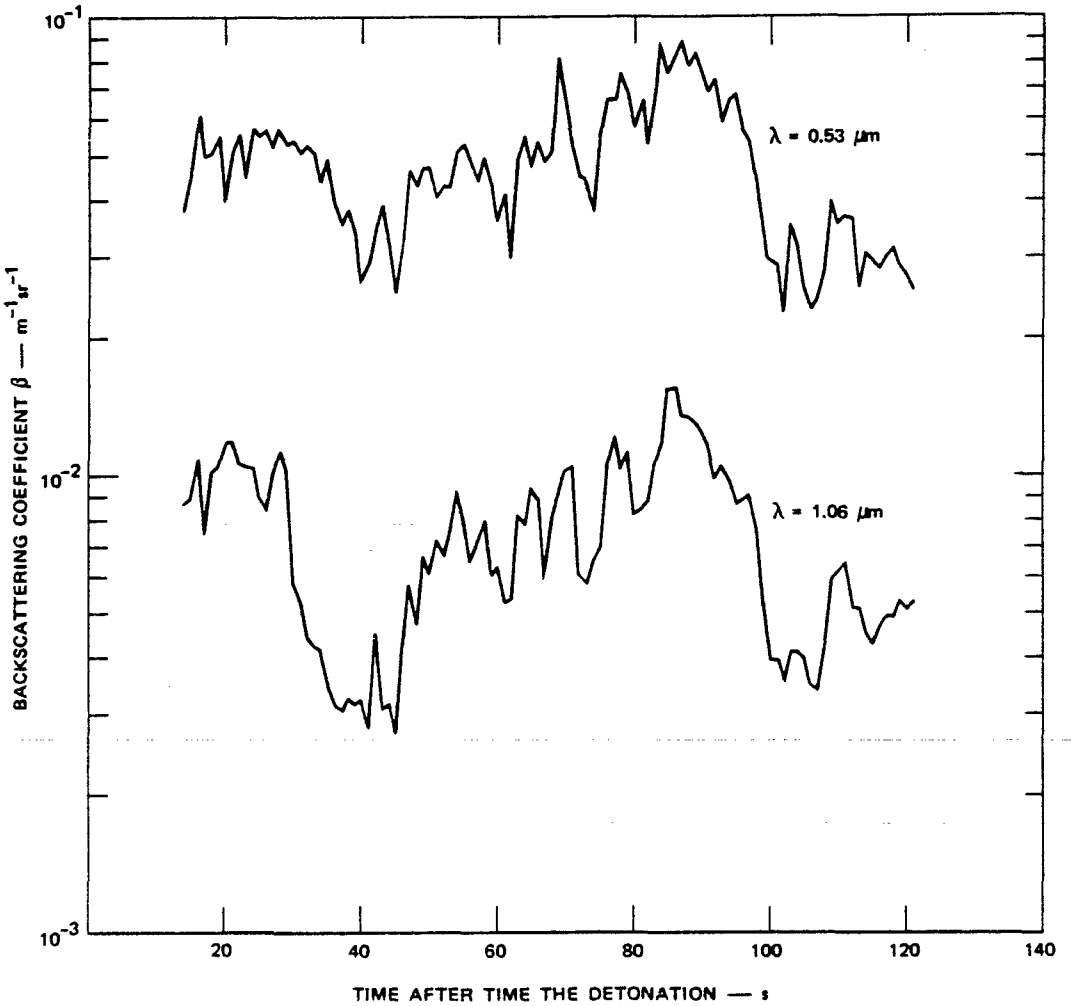

FIGURE 14 AVERAGE BACKSCATTERING COEFFICIENT AT 0.53 AND 1.06 μm AS A FUNCTION OF TIME IMMEDIATELY AFTER THE DETONATION

The calculated backscattering coefficient β is shown in Figure 14 as a function of time after detonation. We have extended the calculation to T + 2 min and have used the tallest peak in cases where more than one peak occurs. The curve presents a value for β averaged over all the values calculated for each interval of 1 s. The slow variation of β with time represents the change of the density of the scattering particle of the front edge of the cloud as it drifts in a north-northwesterly direction that is almost perpendicular to the direction of the laser beam (see Figure 7). The broad maxima may reflect an increased density of the scatterers in the part of the cloud that was created in close vicinity of the explosive charge. Close to two minutes after the detonation the movement of the main cloud indicates that the portion of the cloud formed predominantly by charge No. 5 has passed the laser beam. After that time the value of β decreases and the penetration of the laser beam into the cloud increases slowly.

The value of β at 0.53 μm is on the average about a factor of six larger than at 1.06 μm. This ratio may be too large because, as Figure 6 shows, the pulse at 1.06 μm is truncated by the sampling process. On the average this might increase the value of β at 1.06 μm by a factor of about 1.5, which results in a value for β at 0.53 μm of about four times that at 1.06 μm. This rapid increase of β with λ^{-1} suggests that we are dealing with scattering particles of submicron size, a contention supported by the observation of the haze that produced the scattering during the period from T + 3 min to T + 4 min.

VI SUMMARY AND CONCLUSIONS

This report describes the evaluation and analysis of the data collected with the lidar system at the wavelengths 0.53, 1.06, and 10.6 μm during MB II-2. A problem with a video switch and its associated circuitry prevented recording of the data at 10.6 μm and destroyed the data that contained information about the laser output power and the position of the telescope. The loss of the two last items does not have any significant effect on the analysis presented. The major limitation of the analysis is caused by the unexpectedly small width of the lidar return signal that rendered the 2.5-MHz receiver bandwidth inadequate for fully resolving the signal. The data suggest that the laser beam at 1.06 and 0.53 μm penetrated at most 20 to 100 m into the cloud. During much of the first two minutes after the detonation the penetration may have been significantly less than 20 m because the pulse shape of the return signal was almost identical to the impulse response of the lidar receiver.

To allow transmission measurements a retroreflector array was placed atop Black Mesa. During the first four minutes the laser beam was aimed at this reflector with the beam passing near GZ. The first return signal from the cloud was observed at T + 13 s. Half a second later the signal from the retroreflector disappeared and did not appear again until three minutes later when the main cloud had drifted away from the laser beam. At this time the return signal had become broader and was 20 dB smaller than at the beginning of the event. In many cases the signal consisted of two or three overlapping pulses.

During the entire four minutes that the lidar was aimed at the reflector, the range of the return signals was relative constant varying between 4.7 and 5.0 km. The constancy of the range is attributed to a drift of the cloud in a direction perpendicular to the direction of the laser beam. After T + 4 min the cloud was scanned manually; the pulse shape of the signal remained approximately the same as that observed

when the cloud drifted past the laser beam showing that at 1.06 and 0.53 μm the outer region of the cloud is about the same everywhere. Attempts after T + 8 min to continue measurements of the drifting cloud by using a helicopter that was outfitted with a retroreflector was not successful because of problems with the tracking system and the small penetration of the laser into the cloud.

Before the experimental data were processed, a theory was developed for calculating the volume backscattering coefficient, β. The theory is based on the radar-range equation and the assumption that extinction coefficient is proportional to β. Although the theory is presented in its entirety, most of it was actually not used in the analysis because the width of the return signal was of the same order of magnitude as that of the receiver impulse response.

The analysis is limited to data that were collected during the first two minutes after the detonation. An average value of β is calculated based on calibration data from a target of known reflectance. The range of the calculated values of β is 2 to 9 x 10^{-2} m^{-1} sr^{-1} at 0.53 μm and 3 to 15 x 10^{-3} m^{-1} sr^{-1} at 1.06 μm. The corresponding ranges of reflectance values are from 9 to 42 x 10^{-2} and from 1.4 to 7.10^{-2}, respectively. These remarkably high values are comparable to those obtained from many rough solid surfaces. The wavelength dependence of β indicates that the scattering centers are of submicron size, a fact corroborated by observation of a haze after the main cloud had disappeared, but with the scattering centers still present.

The data show that lasers with the wavelength in the range from 1.06 to 0.53 μm would be completely inoperative in a dust environment such as that created by MBII-2, a result that is not too surprising. However, the small penetration of the laser beam into the cloud was unexpected. It is unfortunate that the 10.6-μm data were lost because we expect that any system using this wavelength would fare significantly better. Even after the main cloud had disappeared scattering particles were still present for a few minutes that could trouble most systems.

It is equally clear that these types of lidar measurements are not well-suited for investigation of cloud formation with particle densities as high as those developed during MBII-2. Extinction coefficients at 0.53 and 1.06 μm were so high that it was not possible to make cross-section per unit volume estimates without making certain assumptions that may not be very realistic.

The lidar signals did not penetrate very deeply into the dust clouds until dust densities fell to very low levels. This is consistent with the appearance of the clouds, which seem "hard" at early times, but become a diffuse haze much later. Measured reflectance values at early times were indeed similar to those from many solid rough, diffusely-reflecting surfaces. Within our ability to resolve range, those echoes also could not be distinguished from ones coming off a solid surface. This means that it would be appropriate to treat many parts of a dust cloud produced by a nuclear or conventional explosion as a solid object in estimating their effects on laser-based military systems.

REFERENCES

1. A. A. Burns, "MISERS BLUFF Electromagnetic Propagation Experiments: Preliminary Results of the UHF-EHF Radar Scattering and Coherent Transmission Experiments," Topical Report, Report No. DNA 4806T-3, Contracts DNA001-77-C-0269 and DNA001-79-C-0181, SRI Projects Nos. 6462 and 4279, SRI International, Menlo Park, California (October 1979).

2. R. S. Vickers, "Medium Frequency Propagation Experiment at MISERS BLUFF," Report No. DNA4806T-1, Contract No. DNA001-77-C-0269, SRI Project No. 6462, SRI International, Menlo Park, California (November 1978).

3. J. G. Hawley and A. A. Burns, "MISERS BLUFF Electromagnetic Propagation Experiments: Preliminary Results of the Laser Experiment," Topical Report, Report No. DNA 4806T-2, Contracts DNA001-77-C-0269 and DNA001-79-C-0181, SRI Projects Nos. 6462 and 8279, SRI International, Menlo Park, California (October 1979).

4. W. L. Wolf and George Zissis (eds.), The Infrared Handbook, "Chapter 23" (IRIS Center, Environmental Research Institute of Michigan, 1978).

5. P. A. Davis, "The Analysis of Lidar Signatures of Cirrus Clouds," Appl. Optics, Vol. 8, No. 10, pp. 2099-2102 (October 1969).

6. F. G. Fernald et al., "Determination of Aerosol Height Distributions by Lidar," J. Appl. Meteor., Vol. 11, No. 3, pp. 482-489 (April 1972).

BLANK PAGE

Appendix A

SOLUTION OF THE RICCATI EQUATION

In Section III the equation [Eq. (12)] for finding $\beta(R)$ was found to be the Riccati equation given by

$$\beta' = f(R)\beta + 2k\beta^2 \tag{A-1}$$

where the apostrophe denotes differentiation with respect to R, and where f(R) is given by

$$f(R) = \frac{dx(R)}{x(R)dR} \quad . \tag{A-2}$$

In these equations R is limited to the range where $x(R) \neq 0$, i.e., the range of the scattering centers. Moving the term $f(R)\beta$ to the left side of Eq. (A-1) and multiplying both sides of the equation by $\exp[-g(R)]$ where

$$g(R) = \int_{R_o}^{R} f(r)dr \tag{A-3}$$

we obtain

$$[\beta' - f(R)\beta] \exp[-g(R)] = 2k\beta^2 \exp[-g(R)] \quad . \tag{A-4}$$

Eq. (A-4) can be written as

$$\{\beta \exp[-g(R)]\}' = 2k\beta^2 \exp[-g(R)] \tag{A-5}$$

or,

$$u' = 2ku^2 \exp[g(R)] \tag{A-6}$$

where

$$u = \beta \exp [-g(R)] \quad . \tag{A-7}$$

From Eq. (A-6) we have

$$\frac{u'}{u^2} = 2k \exp [g(R)] \tag{A-8}$$

that is identical to

$$-\left(\frac{1}{u}\right)' = 2k \exp [g(R)] \quad . \tag{A-9}$$

Eq. (A-9) has the solution

$$-\frac{1}{u} = 2k \int_{R_o}^{R} \exp [g(r)]dr + c \tag{A-10}$$

where c is a constant. From Eqs. (A-7) and (A-10) we obtain,

$$\beta = -\frac{\exp [g(R)]}{2k \int_{R_o}^{R} \exp [g(r)]dr + c} \quad . \tag{A-11}$$

From Eqs. (A-2) and (A-3)

$$g(R) = \ln \frac{x(R)}{x(R_o)} \tag{A-12}$$

so that

$$\beta(R) = -\frac{x(R)/x(R_o)}{2k \int_{R_o}^{R} x(R)/x(R_o) + c} \quad . \tag{A-13}$$

The integration constant c is seen to be

$$c = 1/\beta(R_o) \tag{A-14}$$

by setting $R = R_o$ in Eq. (A-13). Using the expression for x(R) in Eq. (11), the final expression for $\beta(R)$ is,

$$\beta(R) = \frac{\frac{P_r(R)}{P_r(R_o)}\left(\frac{R}{R_o}\right)^2}{1/\beta(R_o) - 2k\int_{R_o}^{R}\frac{P_r(r)}{P_r(R_o)}\left(\frac{r}{R_o}\right)^2 dr} \quad . \tag{A-15}$$

BLANK PAGE

Appendix B

DERIVATION OF EXPRESSION FOR k

Differentiating Eq. (14) with respect to R and solving it for $\beta(R)$ yields

$$\beta(R) = -\frac{1}{2kT^2(R)}\frac{dT^2(R)}{dR} \tag{B-1}$$

Using this expression in Eq. (6) we obtain

$$dT^2(R) = 2k\beta_o \frac{P_r(R)}{P_r\left(R_{cal}\right)}\left(\frac{R}{R_{cal}}\right)^2 T_a^2\left(R_{cal}\right)dR \tag{B-2}$$

where we have used

$$T^2(R) = T_a^2\left(R_{cal}\right)T^2\left(R, R_{cal}\right) \tag{B-3}$$

consistent with the notation used in Eqs. (5) and (7). If we assume that the scattering events are confined to the range $R_o \le R \le R_1$ we obtain the following expression for k by integration of Eq. (B-2),

$$k = \frac{1 - T^2(R_1, R_o)}{2\beta_o T_a^2(R_{cal})\displaystyle\int_{R_o}^{R_1} \frac{P_r(r)}{P_r(R_{cal})}\left(\frac{r}{R_{cal}}\right)^2 dr} \tag{B-4}$$

If the transmittance is measured over the range $0 \le R \le R_2$ where $R_2 > R$, we must use the following relationship in Eq. (4) to find k:

$$T^2\left(R_2\right) = T_a^2\left(R_o\right)T^2\left(R_1, R_o\right)T_a^2\left(R_2, R_1\right) \tag{B-5}$$

where $T_a^2(R_o)$ and $T_a^2(R_2,R_1)$ account for the air transmittance in the part of the range $0 \leq R \leq R_2$ that is free of scattering centers. If the air transmittance over the whole range R_2 is also measured, then

$$T^2(R_1,R_o) = T_a^2(R_1,R_o)\left(\frac{T(R_2)}{T_a(R_2)}\right)^2 \qquad \text{(B-6)}$$

or in terms of received power

$$T^2(R_1,R_o) = T_a^2(R_1,R_o)\,\frac{P_r(R_2)}{P_{r,a}(R_2)} \qquad \text{(B-7)}$$

where $P_{r,a}(R_2)$ is the power received when no scatters are present in the range $0 \leq R \leq R_2$.

DISTRIBUTION LIST

DEPARTMENT OF DEFENSE

Assistant Secretary of Defense
Comm, Cmd, Cont & Intell
ATTN: Dir of Intelligence Sys, J. Babcock

Assistant to the Secretary of Defense
Atomic Energy
ATTN: Executive Asst

Command & Control Technical Ctr
ATTN: C-650, G. Jones
ATTN: C-312, R. Mason
3 cy ATTN: C-650, W. Heidig

Defense Communications Agency
ATTN: Code 480, F. Dieter
ATTN: Code 480
ATTN: Code 205
ATTN: Code 101B

Defense Communications Engineer Center
ATTN: Code R410, J. McLean
ATTN: Code R410, N. Jones
ATTN: Code R123

Defense Intelligence Agency
ATTN: DT-1B
ATTN: DB-4C, E. O'Farrell
ATTN: DB, A. Wise
ATTN: DIR
ATTN: DC-7B

Defense Nuclear Agency
ATTN: NAFD
ATTN: NATD
ATTN: STNA
ATTN: RAEE
3 cy ATTN: RAAE
4 cy ATTN: TITL

Defense Technical Info Ctr
12 cy ATTN: DD

Field Command
Defense Nuclear Agency
ATTN: FCPR, J. T. McDaniel

Field Command
Defense Nuclear Agency
ATTN: FCPRL

Interservice Nuclear Weapons School
ATTN: TTV

Joint Chiefs of Staff
ATTN: C3S, Evaluation Office
ATTN: C3S

Joint Strat Tgt Planning Staff
ATTN: JLA
ATTN: JLTW-2

National Security Agency
ATTN: B-3, F. Leonard
ATTN: W-32, O. Bartlett
ATTN: R-52, J. Skillman

DEPARTMENT OF DEFENSE (Continued)

Under Secretary of Def for Rsch & Engrg
ATTN: Defensive Systems
ATTN: Strategic & Space Sys (OS)

WWMCCS System Engineering Org
ATTN: J. Hoff

DEPARTMENT OF THE ARMY

Assistant Chief of Staff for Automation & Comm
Department of the Army
ATTN: DAAC-ZT, P. Kenny

Atmospheric Sciences Lab
U.S. Army Electronics R&D Command
ATTN: DELAS-EO, F. Niles
ATTN: DELAS-AS, H. Holt

BMD Advanced Technology Ctr
Department of the Army
ATTN: ATC-T, M. Capps

BMD Systems Command
Department of the Army
2 cy ATTN: BMDSC-HW

Deputy Chief of Staff for Ops & Plans
Department of the Army
ATTN: DAMO-RQC

Harry Diamond Laboratories
Department of the Army
ATTN: DELHD-TA-L
ATTN: DELHD-NW-R, R. Williams
ATTN: DELHD-NW-P

U.S. Army Chemical School
ATTN: ATZN-CM-CS

U.S. Army Comm-Elec Engrg Instal Agency
ATTN: CCC-CED-CCO, W. Neuendorf
ATTN: CCC-EMEO-PED, G. Lane

U.S. Army Communications Command
ATTN: CC-OPS-W
ATTN: CC-OPS-WR, H. Wilson

U.S. Army Communications R&D Command
ATTN: DRDCO-COM-RY, W. Kesselman

U.S. Army Foreign Science & Tech Ctr
ATTN: DRXSI-SD

U.S. Army Materiel Dev & Readiness Cmd
ATTN: DRCLDC, J. Bender

U.S. Army Missile Command
2 cy ATTN: Redstone Scientific Info Ctr

U.S. Army Missile Intelligence Agency
ATTN: YSE, J. Gamble

U.S. Army Nuclear & Chemical Agency
ATTN: Lib

DEPARTMENT OF THE ARMY (Continued)

U.S. Army Satellite Comm Agency
ATTN: Document Control

U.S. Army TRADOC Sys Analysis Actvy
ATTN: ATAA-TDC
ATTN: ATAA-PL
ATTN: ATAA-TCC, F. Payan Jr

DEPARTMENT OF THE NAVY

COMSPTEVFOR
Department of the Navy
ATTN: Code 605, R. Berg

Joint Cruise Missiles Project Ofc
Department of the Navy
ATTN: JCMG-707

Naval Air Development Center
ATTN: Code 6091, M. Setz

Naval Air Systems Command
ATTN: PMA 271

Naval Electronics Systems Command
ATTN: PME 117-211, B. Kruger
ATTN: PME 106-13, T. Griffin
ATTN: PME 117-2013, G. Burnhart
ATTN: PME 117-20
ATTN: Code 3101, T. Hughes
ATTN: Code 501A
ATTN: PME 106-4, S. Kearney

Naval Intelligence Support Ctr
ATTN: NISC-50

Naval Ocean Systems Center
ATTN: Code 5322, M. Paulson
ATTN: Code 532, J. Bickel
ATTN: Code 532, R. Pappert
3 cy ATTN: Code 5323, J. Ferguson

Naval Research Lab
ATTN: Code 6730, E. McClean
ATTN: Code 7550, J. Davis
ATTN: Code 4780, S. Ossakow
ATTN: Code 7950, J. Goodman
ATTN: Code 4700, T. Coffey
ATTN: Code 7500, B. Wald
ATTN: Code 4701, J. Brown
ATTN: Code 5300
ATTN: Code 4187
ATTN: Code 2627

Naval Space Surveillance System
ATTN: J. Burton

Naval Surface Weapons Ctr
ATTN: Code F31

Office of Naval Research
ATTN: Code 420
ATTN: Code 421

Office of the Chief of Naval Operations
ATTN: OP 65
ATTN: OP 981N
ATTN: OP 941D

DEPARTMENT OF THE NAVY (Continued)

Naval Telecommunications Command
ATTN: Code 341

Strategic Systems Project Office
Department of the Navy
ATTN: NSP-43
ATTN: NSP-2722, F. Wimberly
ATTN: NSP-2141

DEPARTMENT OF THE AIR FORCE

Aerospace Defense Command
Department of the Air Force
ATTN: DC, T. Long

Air Force Geophysics Lab
ATTN: PHP
ATTN: OPR-1
ATTN: LKB, K. Champion
ATTN: OPR, A. Stair
ATTN: PHI, J. Buchau
ATTN: R. Thompson
ATTN: S. Basu

Air Force Weapons Lab
Air Force Systems Command
ATTN: SUL
ATTN: CA
ATTN: NTYC
ATTN: NTN

Air Force Wright Aeronautical Lab
ATTN: A. Johnson
ATTN: W. Hunt

Air Logistics Command
Department of the Air Force
ATTN: OO-ALC/MM

Air University Library
Department of the Air Force
ATTN: AUL-LSE

Air Weather Service, MAC
Department of the Air Force
ATTN: DNXP, R. Babcock

Assistant Chief of Staff
Studies & Analyses
Department of the Air Force
ATTN: AF/SASC, W. Keaus
ATTN: AF/SASC, C. Rightmeyer

Ballistic Missile Office
Air Force Systems Command
ATTN: ENBE
ATTN: PM
ATTN: HQ Space DIV/RSP
ATTN: ENSN, J. Allen

Deputy Chief of Staff
Operations Plans and Readiness
Department of the Air Force
ATTN: AFXOKS
ATTN: AFXOKCD
ATTN: AFXOXFD
ATTN: AFXOKT

DEPARTMENT OF THE AIR FORCE (Continued)

Deputy Chief of Staff
Rsch, Development, & Acq
Department of the Air Force
ATTN: AFRDSS
ATTN: AFRDSP
ATTN: AFRDS

Electronic Systems Div
Department of the Air Force
ATTN: DCKC, J. Clark

Electronic Systems Div
Department of the Air Force
ATTN: OCT-4, J. Deas

Electronic Systems Div
Department of the Air Force
ATTN: YSEA
ATTN: YSM, J. Kobelski

Foreign Technology Div
Air Force Systems Command
ATTN: TQTD, B. Ballard
ATTN: NIIS, Lib

Rome Air Development Ctr
Air Force Systems Command
ATTN: TSLD
ATTN: OCS, V. Coyne

Rome Air Development Ctr
Air Force Systems Command
ATTN: EEP

Space Div
Department of the Air Force
ATTN: SKY, C. Kennedy
ATTN: SKA, D. Bolin

Space Div
Department of the Air Force
ATTN: YGJB, W. Mercer
ATTN: YGJ

Space Div
Department of the Air Force
ATTN: E. Butt

Strategic Air Command
Department of the Air Force
ATTN: DCX
ATTN: XPFS
ATTN: XPFS, B. Stephan
ATTN: DCXT
ATTN: ADWATE, B. Bauer
ATTN: NRT
ATTN: DCXR, T. Jorgensen

OTHER GOVERNMENT AGENCIES

National Bureau of Standards
ATTN: Sec Ofc for R. Moore

National Oceanic & Atmospheric Admin
Environmental Research Labs
ATTN: R. Grubb
ATTN: D. Williams

OTHER GOVERNMENT AGENCIES (Continued)

Institute for Telecommunications Sciences
National Telecommunications & Info Admin
ATTN: L. Berry
ATTN: W. Utlaut
ATTN: A. Jean

DEPARTMENT OF ENERGY

EG&G, Inc
Los Alamos Div
ATTN: D. Wright
ATTN: J. Colvin

DEPARTMENT OF ENERGY CONTRACTORS

Lawrence Livermore National Lab
ATTN: L-96, T. Donich
ATTN: Tech Info Dept Lib

Los Alamos National Lab
ATTN: G-6, E. Jones
ATTN: C. Westervelt
ATTN: R. Taschek
ATTN: MS 668, J. Malik
ATTN: P. Keaton

Sandia National Labs
Livermore Lab
ATTN: T. Cook
ATTN: B. Murphey

Sandia National Lab
ATTN: D. Dahlgren
ATTN: D. Thornbrough
ATTN: C. Williams
ATTN: C. Mehl
ATTN: Space Project Div
ATTN: ORG 1250, W. Brown
ATTN: 3141

DEPARTMENT OF DEFENSE CONTRACTORS

Aerospace Corp
ATTN: G. Anderson
ATTN: I. Garfunkel
ATTN: D. Olsen
ATTN: L. Straus
ATTN: V. Josephson
ATTN: S. Bower
ATTN: T. Salmi
ATTN: N. Stockwell
ATTN: R. Slaughter
ATTN: A. Morse
ATTN: W. Grabowsky

Analytical Systems Engineering Corp
ATTN: Radio Sciences

Analytical Systems Engineering Corp
ATTN: Security

Barry Rsch Corp
ATTN: J. McLaughlin

BDM Corp
ATTN: L. Jacobs
ATTN: T. Neighbors

DEPARTMENT OF DEFENSE CONTRACTORS (Continued)

Berkeley Research Associates, Inc
ATTN: J. Workman

BETAC
ATTN: J. Hirsch

Boeing Co
ATTN: S. Tashird
ATTN: G. Hall
ATTN: M/S 42-33, J. Kennedy

Booz-Allen & Hamilton, Inc
ATTN: B. Wilkinson

University of California at San Diego
ATTN: H. Booker

Charles Stark Draper Lab, Inc
ATTN: J. Gilmore
ATTN: D. Cox

Communications Satellite Corp
ATTN: D. Fang

Computer Sciences Corp
ATTN: F. Eisenbarth

Comsat Labs
ATTN: G. Hyde

Cornell University
ATTN: M. Kelly
ATTN: D. Farley Jr

E-Systems, Inc
ATTN: R. Berezdivin

Electrospace Systems, Inc
ATTN: H. Logston
ATTN: P. Phillips

ESL, Inc
ATTN: J. Marshall

General Electric Co
ATTN: R. Edsall
ATTN: A. Harcar

General Electric Co
ATTN: A. Steinmayer
ATTN: C. Zierdt

General Electric Co
ATTN: G. Millman
ATTN: F. Reibert

General Electric Co
ATTN: G. Millman

General Research Corp
ATTN: J. Garbarino
ATTN: J. Ise Jr

Horizons Technology, Inc
ATTN: R. Kruger

HSS, Inc
ATTN: D. Hansen

DEPARTMENT OF DEFENSE CONTRACTORS (Continued)

IBM Corp
ATTN: F. Ricci

University of Illinois
ATTN: Sec Supervisor for K. Yeh

Information Science, Inc
ATTN: W. Dudziak

Institute for Defense Analyses
ATTN: E. Bauer
ATTN: H. Wolfhard
ATTN: J. Aein

International Tel & Telegraph Corp
ATTN: Tech Lib
ATTN: G. Wetmore

JAYCOR
ATTN: J. Sperling

JAYCOR
ATTN: J. Doncarlos

Johns Hopkins University
ATTN: T. Potemra
ATTN: J. Phillips
ATTN: T. Evans
ATTN: J. Newland
ATTN: P. Komiske

Kaman Sciences, Inc
ATTN: N. Beauchamp
ATTN: F. Foxwell

Kaman Tempo
ATTN: K. Schwartz
ATTN: W. Knapp
ATTN: T. Stephens
ATTN: DASIAC

Linkabit Corp
ATTN: I. Jacobs

Litton Systems, Inc
ATTN: R. Grasty

Lockheed Missiles & Space Co, Inc
ATTN: R. Johnson
ATTN: M. Walt
ATTN: R. Au
ATTN: W. Imhof

Lockheed Missiles & Space Co, Inc
ATTN: D. Churchill
ATTN: Dept 60-12
ATTN: C. Old

M.I.T. Lincoln Lab
ATTN: D. Towle
ATTN: J. Evans

Martin Marietta Corp
ATTN: R. Hefner

Meteor Communications Consultants
ATTN: R. Leader

DEPARTMENT OF DEFENSE CONTRACTORS (Continued)

McDonnell Douglas Corp
ATTN: R. Halprin
ATTN: W. Olson
ATTN: G. Mroz
ATTN: J. Moule
ATTN: N. Harris

Mission Research
ATTN: C. Longmire
ATTN: Tech Lib
ATTN: F. Fajen
ATTN: M. Scheibe
ATTN: R. Bogusch
ATTN: R. Hendrick
ATTN: R. Kilb
ATTN: S. Gutsche

Mitre Corp
ATTN: B. Adams
ATTN: C. Callahan
ATTN: A. Kymmel
ATTN: G. Harding

Mitre Corp
ATTN: M. Horrocks
ATTN: W. Hall
ATTN: W. Foster

Pacific-Sierra Research Corp
ATTN: F. Thomas
ATTN: E. Field Jr
ATTN: H. Brode

Pennsylvania State University
ATTN: Ionospheric Research Lab

Photometrics, Inc
ATTN: I. Kofsky

Physical Dynamics, Inc
ATTN: E. Fremouw

Physical Research, Inc
ATTN: R. Deliberis

R & D Associates
ATTN: C. Greifinger
ATTN: F. Gilmore
ATTN: H. Ory
ATTN: R. Turco
ATTN: R. Lelevier
ATTN: W. Wright
ATTN: W. Karzas
ATTN: M. Gantsweg
ATTN: B. Gabbard
ATTN: P. Haas

R & D Associates
ATTN: B. Yoon

Rand Corp
ATTN: E. Bedrozian
ATTN: C. Crain

Raytheon Co
ATTN: G. Thome

DEPARTMENT OF DEFENSE CONTRACTORS (Continued)

Riverside Research Institute
ATTN: V. Trapani

Rockwell International Corp
ATTN: R. Buckner

Rockwell International Corp
ATTN: S. Quilici

Santa Fe Corp
ATTN: D. Paolucci

Science Applications, Inc
ATTN: L. Linson
ATTN: D. Sachs
ATTN: C. Smith
ATTN: E. Straker
ATTN: D. Hamlin
ATTN: R. Lee

Science Applications, Inc
ATTN: SZ

SRI International
ATTN: W. Jaye
ATTN: J. Depp
ATTN: G. Smith
ATTN: A. Burns
ATTN: G. Price
ATTN: R. Tsunoda
ATTN: R. Leonard
ATTN: R. Livingston
ATTN: W. Chesnut
ATTN: R. Leadabrand
ATTN: D. Neilson
ATTN: M. Baron
ATTN: J. Petrickes
ATTN: C. Rino
4 cy ATTN: A. Rosengreen

SRI International
ATTN: F. Perkins

Sylvania Systems Group
ATTN: R. Steinhoff
ATTN: I. Kohlberg

Teledyne Brown Engineering
ATTN: N. Passino

TRI-COM, Inc
ATTN: D. Murray

TRW Defense & Space Sys Group
ATTN: R. Plebuch
ATTN: D. Dee

Utah State University
ATTN: K. Baker
ATTN: J. Dupnik
ATTN: L. Jensen

Visidyne, Inc
ATTN: J. Carpenter